AN OVERVIEW OF HOT GAS INGESTION RESEARCH AT THE UNIVERSITY OF BATH

J.A. Scobie - C.M. Sangan - J.M. Owen - G.D. Lock

Department of Mechanical Engineering, University of Bath, Bath, United Kingdom, BA2 7AY.

j.a.scobie@bath.ac.uk

ABSTRACT

   Rim seals are fitted in gas turbines at the periphery of the wheel-space formed between rotor discs and their adjacent casings. These seals reduce the ingestion of hot gases that can cause significant damage to some of the most highly stressed components in the engine. In gas turbine engines this ingestion is principally caused by circumferential pressure asymmetries in the mainstream annulus, radially outward of the rim seal. A superposed sealant flow, bled from the compressor, is used to reduce or, at the limit, prevent ingestion. As the use of this sealing air can reduce the cycle efficiency, it is important to know how much flow is required to prevent ingestion and to understand the associated fluid dynamics and heat transfer when ingestion occurs.

   This paper presents an overview of experimental results from a research facility which models an axial turbine stage with generic, but engine-representative, rim seals. Measurements of pressure, gas concentration, temperature and swirl are used to assess the performance of different seal designs. As ingestion through the rim seal is a consequence of an unsteady, three-dimensional flow field, the cause-effect relationship between pressure and the sealing effectiveness is complex. The approach at Bath has been to conduct fundamental work to measure and understand the fluid dynamics using generic, fully-instrumented experiments specifically designed for the available measurement techniques. The experimental data is shown to be successfully calculated by simple effectiveness equations developed from a series of theoretical models which can be used to aid the design of more specific engine geometries.

NOMENCLATURE

b	characteristic radius of seal
$C_{d,e}$ $C_{d,i}$	discharge coefficients for egress, ingress
C_p	pressure coefficient [$= p\text{-}p_{ref} / (^1\!/_2\rho\Omega^2 b^2)$]
C_w	non-dimensional flow rate [$= \dot{m} / \mu b$]
$C_{w,0}$	non-dimensional sealing flow rate
$C_{w,min}$	minimum value of $C_{w,0}$ to prevent ingress
c	concentration
G	gap ratio [$= S / b$]
G_c	seal-clearance ratio [$= s_c / b$]
g	normalised pressure difference across seal [$= p_1\text{-}p_{2,min} / p_{2,max}\text{-}p_{2,min}$]
$\dot{m}$	mass flow rate
p	absolute static pressure
r	radius
Re_w	axial Reynolds number in annulus [$= \rho W b / \mu$]
Re_ϕ	rotational Reynolds number [$= \rho \Omega b^2 / \mu$]
s_c	seal clearance
S	axial clearance between stator and rotor
T	temperature

U	bulk-mean velocity through rim-seal clearance $[= \dot{m} / 2\pi\rho bs_c]$
V_ϕ	tangential component of velocity
W	axial velocity in annulus
z	axial distance
β	swirl ratio in wheel-space $[= V_\phi / \Omega r]$
ΔC_p	non-dimensional pressure difference $[= \Delta p / (^1/_2\rho\Omega^2 b^2)]$
Δp	peak-to-trough pressure difference in annulus $[= p_{max}-p_{min}]$
Γ_c	ratio of discharge coefficients $[= C_{d,i}/ C_{d,e}]$
ε	sealing effectiveness $[= C_{w,0}/ C_{w,e} = \Phi_0 / \Phi_e]$
ε_{ad}	adiabatic effectiveness for rotor $[= (T_{ad} - T_a) / (T_{ad}* - T_a)]$
ε_c	concentration effectiveness $[= (c_s-c_a) / (c_o-c_a)]$
ε_p	pressure effectiveness
Φ	non-dimensional sealing parameter $[= C_w / 2\pi G_c Re_\phi]$
Φ_{min}	value of Φ when $C_w = C_{w,min}$
Φ_0	value of Φ when $C_w = C_{w,0}$
θ	non-dimensional vane pitch
λ_T	turbulent flow parameter $[= C_{w,0}Re_\phi^{-0.8}]$
μ	dynamic viscosity
ρ	density
Ω	angular velocity of rotating disc

Subscripts

|	
a	annulus
e	egress
i	ingress
s	stator
0	superposed flow
ϕ	angular coordinate

INTRODUCTION

Hot gas ingestion in turbine engines is predominately caused by the unsteady three-dimensional variation of pressure in the mainstream flow-path. Ingress and egress will occur in the regions of the seal clearance where the pressure in the annulus is higher or lower than that in the wheel-space, respectively. Sealing air, bled from the compressor, is used to raise the pressure in the wheel-space and reduce or prevent ingress. The use of too much sealing air is inefficient and can cause aerodynamic losses as it exits the rim seal. However, too little can cause overheating and threaten the integrity and operating life of critical components such as rotor discs. The literature related to this topic has been extensively reviewed by Sangan *et al.* (2013a/b) and Sangan *et al.* (2014).

The gas turbine research group at the University of Bath has investigated the effects of ingestion experimentally, theoretically and computationally over the last nine years. This research addresses some of the issues faced by the modern day engine designer; principally it is important to know the following:

1. When ingress occurs, how much hot gas enters the wheel-space and how far does it penetrate?
2. How does ingress affect the flow structure in the wheel-space?
3. How much sealing air is required to prevent ingress and how can this be predicted?
4. What is the most effective seal geometry to prevent ingress?
5. What is the effect of ingress on the temperature of the rotor disc?
6. How can the engine designer relate rig experiments to engine conditions?

This paper presents an overview of the experimental results obtained from the University's single-stage research facility which models ingestion through generic, but engine-representative, rim seals. The results are presented in a format which aims to systematically address each of the questions posed above.

Flow Structure in the Wheel-Space
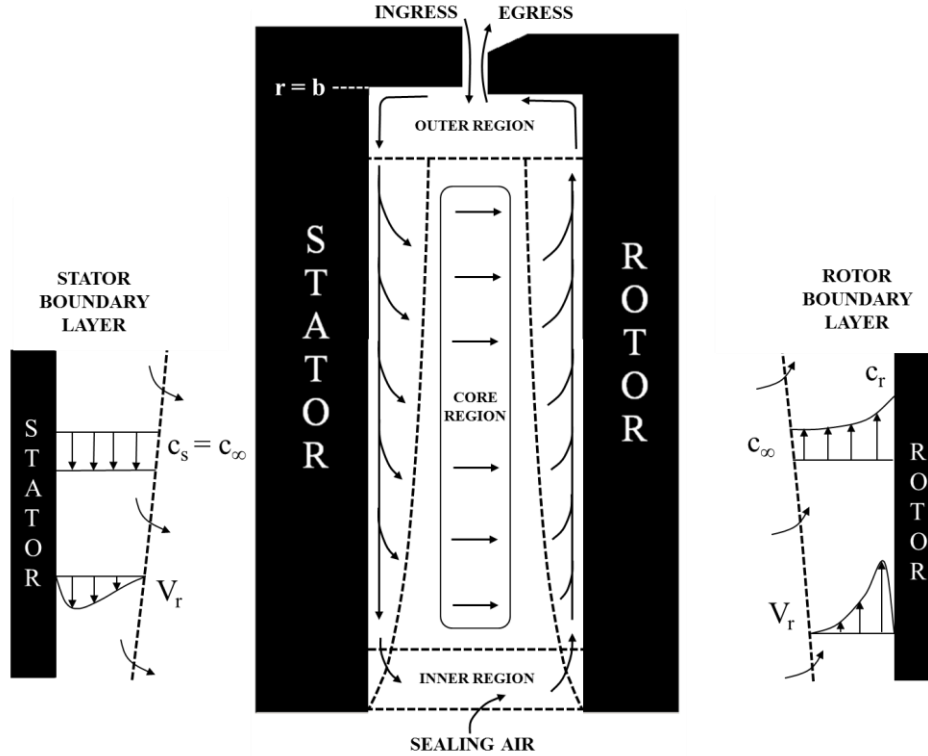
Figure 1: Simplified flow structure diagram showing boundary layers on the stator and rotor

Figure 1 shows the flow structure for a rotor-stator system with superposed sealing flow, together with egress and ingress through the rim seal. The rotational Reynolds number and wheel-space dimensions are such that separate boundary layers form on the two discs. At the rotor surface, fluid is accelerated to the disc speed by friction and pumped centrifugally; on the stationary surfaces the tangential velocity decreases to zero near the wall and the radial pressure gradient causes the fluid to migrate radially inwards. The swirl of the fluid in the inviscid core between the boundary layers controls this radial distribution of static pressure. In a rotating inviscid fluid, the radial component of velocity, and the axial gradients of the axial and tangential components of velocity, must be zero (Owen and Rogers, 1989). All radial flow occurs inside the boundary layers, and the swirl adjusts to satisfy the continuity of the flow rate in the boundary layers.

The superposed sealing flow is entrained into the boundary layer on the rotor within the inner region, the extent of which increases with increasing sealing flow rate. In the outer region ingress and egress combine through mixing in the seal clearance where conservation of mass, angular momentum and energy will determine the resultant swirl, concentration and temperature of the fluid. This region is the source of the flow in the boundary layer on the stator; if the fluid is fully mixed, the concentration (and for an adiabatic stator, the temperature) within the boundary layer on the stator, and that in the adjacent core, will be invariant with radius. Outside the inner and outer regions, fluid leaves the boundary layer on the stator to be entrained by that on the rotor. Consequently, the concentration in the rotor boundary layer will decrease as the flow moves radially outward over the rotor.

Governing Non-Dimensional Parameters for Ingress

The ingress of fluid through the rim seal is an inertial phenomenon driven by differences in pressure, whereas the flow inside the wheel-space is controlled by the boundary layers on the rotor and stator. Defined below are two non-dimensional flow variables (Φ_0 and λ_T) which respectively govern these inviscid and viscous phenomena.

The sealing flow parameter, Φ_0, combines the effects of $C_{w,0}$, G_c, and Re_ϕ into a single flow variable as follows:

$$\Phi_0 = \frac{C_{w,0}}{2\pi G_c \, \mathrm{Re}_\phi} = \frac{U}{\Omega b}$$

where U is the bulk-mean velocity through the rim-seal clearance. As both Re_ϕ and $C_{w,0}$ include viscous terms which cancel, Φ_0 is therefore an inertial parameter.

The structure of the flow in the wheel-space is determined by the turbulent flow parameter, which is defined as:

$$\lambda_T = C_{w,0} \, \mathrm{Re}_\phi^{-0.8}$$

For the free disc, where there is no stator, the entrained flow rate is characterised by $\lambda_T \approx 0.22$. In the wheel-space, values of $\lambda_T > 0.22$ are expected to suppress the core rotation.

For the experiments described below, $Re_\phi \sim 10^6$ and Φ_0 and λ_T are coincidently, nearly equal in magnitude.

Experimental Facility

This section summarises the University of Bath single-stage experimental gas turbine test facility. For a detailed description of this facility the reader is directed towards Sangan *et al.* (2013a).

The 1-stage test rig experimentally simulates hot gas ingestion into the wheel-space of an axial turbine stage. The test section of the facility, shown in Figure 2, features a single turbine stage with 32 vanes and 41 blades. The disc to which the blades were attached could be rotated by an electric motor. To avoid the necessity of a dynamometer to extract excess power, the blades were symmetric NACA 0018 aerofoils.

The vanes and blades, formed from nylon by rapid-prototyping, were secured to aluminium platforms which form the periphery of the stator and rotor respectively. Both the stationary and rotating discs (highlighted in Figure 2) were manufactured from transparent polycarbonate to allow optical access to the wheel-space for the application of thermochromic liquid crystal (TLC). The characteristic radius of the facility, b, measured from the centreline to the inside of the stator shroud was 190 mm.
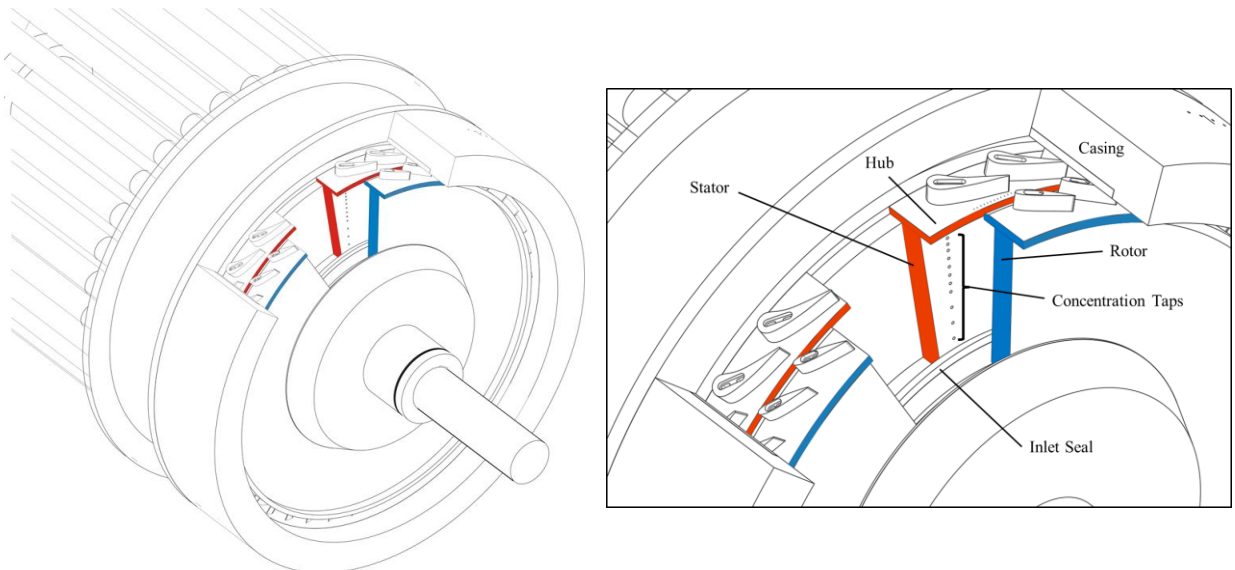
Figure 2: Rig test section (flow is from left to right)

The disc could be rotated up to speeds of 4000 rpm, providing a maximum rotational Reynolds number, Re_ϕ (based on disc radius) up to 1.1×10^6. This value is typically an order-of-magnitude less than that found in gas turbines. However, for rotating flow the turbulent flow structure in the boundary layers is principally governed by the turbulent flow parameter, λ_T, and depends only weakly on Re_ϕ (Owen and Rogers, 1989). Hence the flow structure in the rig is considered to be representative of that found in the cooling systems of engines.

Sealing air was introduced into the wheel-space at a low radius through an annular-shaped inlet seal. For the steady-state concentration measurements, the sealing flow was seeded with CO_2 tracer gas and the variation of concentration with radius determined by sampling through taps along the stator. For the transient heat transfer measurements, the sealing flow was heated by passing it through a thin, wire mesh supplied by an abrupt, controlled surge of electrical current. Both the sealant and external mass flow rates were measured using orifice plates manufactured to EN ISO 5167-2 with an uncertainty of +/- 3%.

Concentration Measurements

For a full description of the CO_2 measurement technique the reader is referred to Sangan *et al.* (2013a). To measure the degree of ingestion, the sealant air was seeded with 1% CO_2 and introduced into the wheel-space at a low radius ($r/b = 0.642$) through an inlet seal. The concentration of CO_2 was monitored at the entrance to the wheel-space, c_0, and in the unseeded upstream flow through the annulus, c_a. The variation of concentration c_s with radius ($0.55 < r/b < 0.993$) along the stator in the wheel-space was determined by sampling through 15 tubes of diameter 1.6 mm (shown in Figure 2). The gas was extracted by a pump, which delivered the samples to an infrared gas analyser.

The concentration sealing effectiveness, ε_c, is defined as

$$\varepsilon_c = \frac{c_s - c_a}{c_o - c_a}$$

It follows that $\varepsilon_c = 1$ when there is no ingress and $\varepsilon_c = 0$ when the sealing flow rate is zero.

Pressure Measurements

Steady pressure measurements were made at various locations in the test rig using a Scanivalve system with Druck PDCR 22 transducers. A series of radial taps in the wheel-space, similar to the concentration taps, were used to determine the static pressure on the stator. Seven complimentary Pitot tubes, aligned with the tangential direction, were used to measure the total pressure in the fluid core. The tangential component of velocity in the core at each location was then calculated from Bernoulli's equation.

The circumferential variation of static pressure in the annulus on the stator shroud hub downstream of the trailing edge of the vane was measured at the design condition by Sangan *et al.* (2013a), and shown to be the driving potential for ingestion. A typical circumferential pressure distribution in the annulus is shown in Figure 3.

A theoretical model was developed by Owen *et al.* (2014) to calculate the axial location where the pressures should be measured on the vane platform in the annulus to ensure consistency between ε_p and ε_c, the effectiveness determined from pressure and concentration respectively. The sealing effectiveness in the model is related to g, the normalized pressure difference across the seal, where

$$g = \frac{p_1 - p_{2,\min}}{p_{2,\max} - p_{2,\min}}$$

The subscripts 1 and 2 refer to the locations in the wheel-space and annulus respectively, as shown in Figure 3. It was shown from the orifice model equations that

$$\varepsilon_p = 1 - \Gamma_c \left[\frac{1-g}{g} \right]^{3/2}$$

In practice, g (and therefore ε_p) depends on the sealing flow rate and where the pressures are measured. At the location of consistency, known as the *sweet spot*, $\varepsilon_p = \hat{\varepsilon}_p$ and $g = \hat{g}$ therefore

$$\widehat{\varepsilon}_p = \varepsilon_c = 1 - \Gamma_c \left[\frac{1 - \widehat{g}}{\widehat{g}} \right]^{3/2}$$
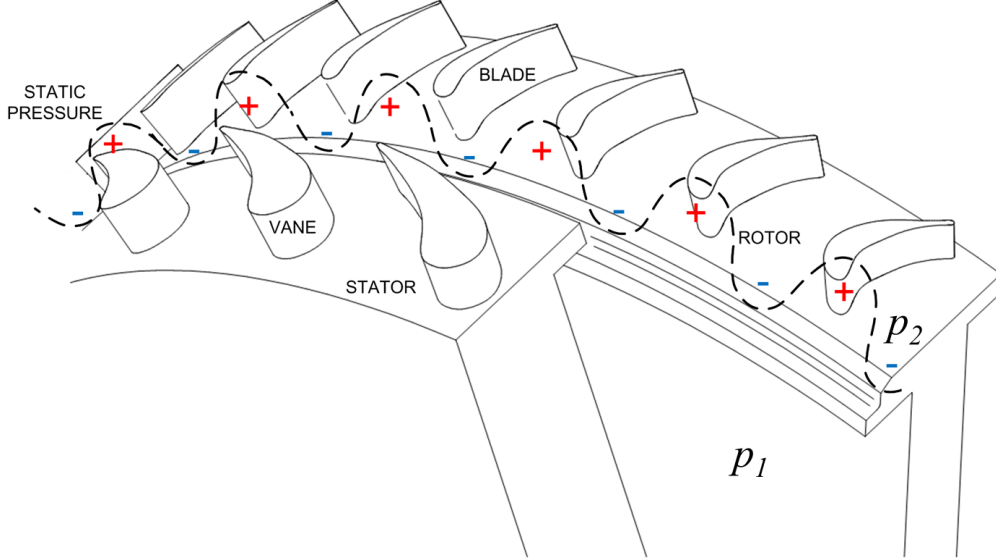
Figure 3: Circumferential pressure distribution in a typical gas turbine engine

TLC Measurements

The adiabatic surface temperatures on the rotor were determined from transient surface-temperature measurements using three narrow band TLCs. The crystals were sprayed onto a segment of the disc and viewed through the transparent polycarbonate by a digital camera. A strobe light was then used to illuminate the TLC and synchronized to the rotor so that the segment was *frozen*.

The adiabatic effectiveness is defined as

$$\varepsilon_{ad} = \frac{T_{ad} - T_a}{T_{ad}^* - T_a}$$

where T_{ad} is the adiabatic surface temperature (where all the bounding solids are perfect insulators), T_{ad}^* the value of T_{ad} when there is no ingress, and T_a is the total temperature of the air in the annulus.

A full description of the TLC measurement technique, including the determination procedure for extracting T_{ad} from measured data, is presented in Pountney *et al.* (2013).

Although it is shown that effectiveness can be measured using several different techniques, it is implicitly assumed that all definitions are equivalent and equal to the theoretical effectiveness, ε, used in the orifice model developed by Owen (2011).

RESULTS

Radial Distribution of Effectiveness
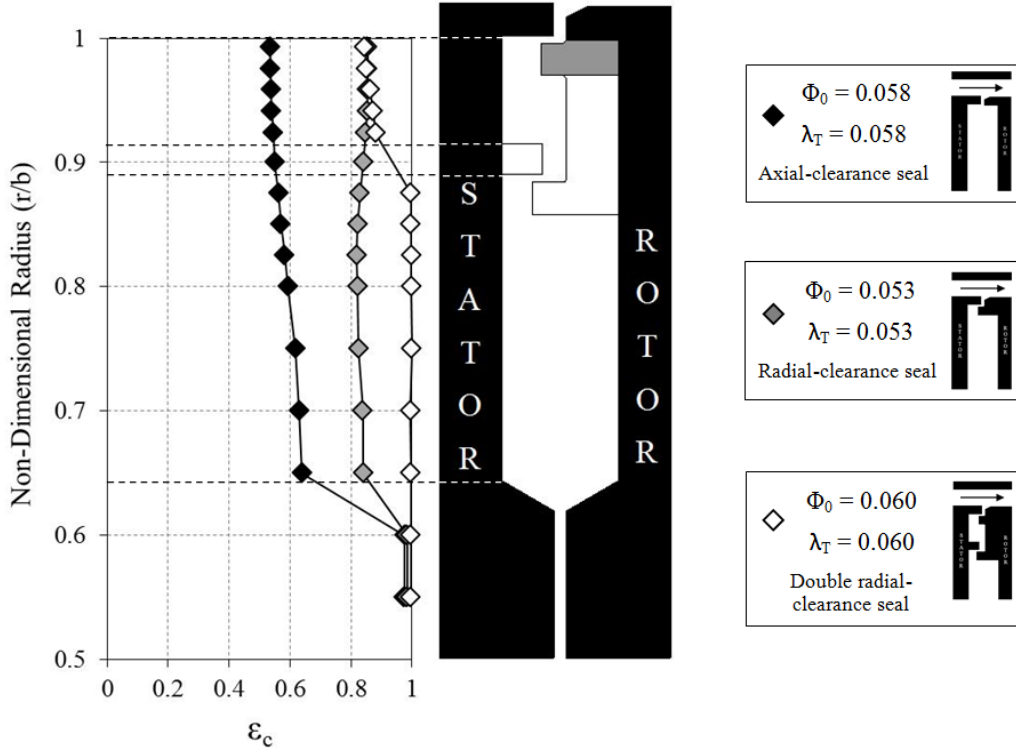
Figure 4: Radial distribution of effectiveness for three seal geometries tested at a consistent sealant flow rate.

Figure 4 shows the radial variation of ε_c on the stator surface for tests at $Re_\phi = 8.17 \times 10^5$. The tests were conducted for each of the rim seals at a consistent sealant flow rate; in all cases ingress occurred. For the single-clearance seals the effectiveness is broadly invariant with radius for $r/b > 0.65$, suggesting that near-complete mixing has occurred in a region very close to the rim-seal. If the flow was not fully mixed then there would be concentration gradients in the stator boundary layer and consequently a radial variation. The rapid increase in ε_c at the smaller radii is caused by the presence of the inner seal, which prevents or strongly reduces the ingestion of fluid into the region where the sealing flow is introduced.

Figure 4 also shows the radial-clearance seal is significantly more effective than the axial-clearance seal at this sealant flow rate. In the outer wheel-space of the double radial-clearance seal ($r/b > 0.913$), the effectiveness is virtually the same as the single seal equivalent for all radial locations. The slight variation of ε_c with r/b is possibly due to the proximity of the radial seal to the stator. In the inner wheel-space of the double seal however, the effectiveness is significantly higher than that of the single seal for the same sealing flow rate. Ingestion is therefore predominantly constrained within the outer wheel-space. In the practical situation of an engine, the inner stator wall could operate at an acceptably low metal temperature with the hot, ingested gas confined to the outer wheel-space protected by a more robust alloy.

For further discussion on the performance of single and double rim seals, including the details of the seal geometries, the reader is directed towards Sangan *et al.* (2013c).

Radial Distribution of Swirl Ratio and Pressure Coefficient
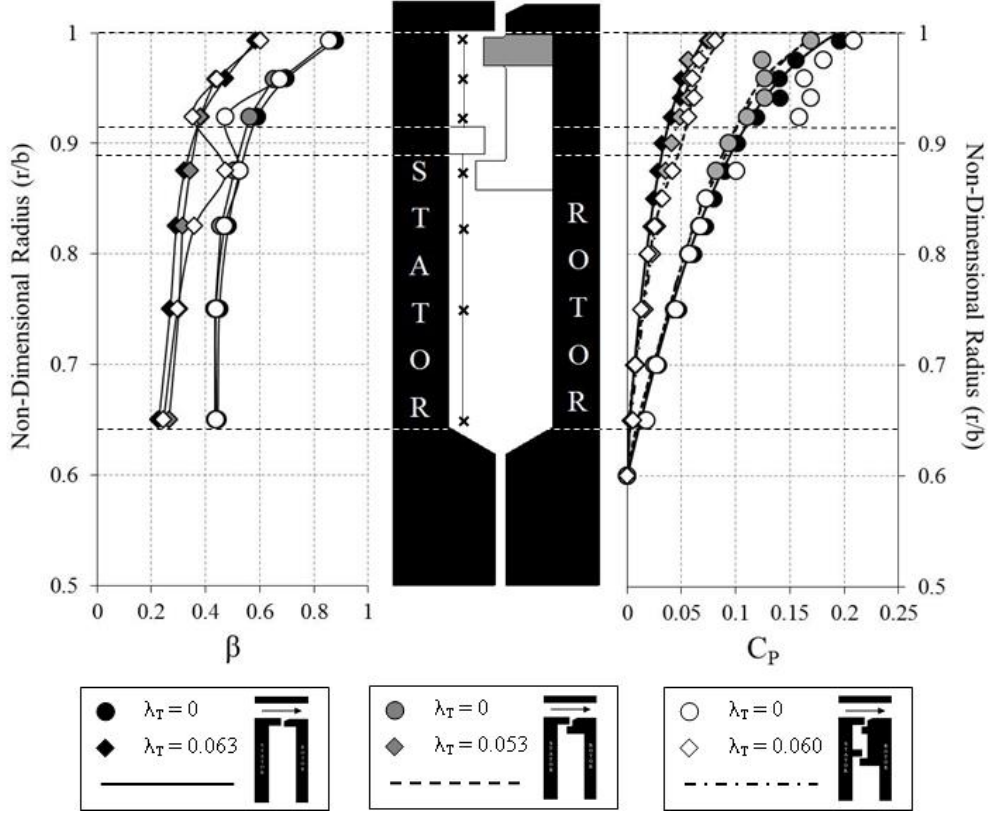
Figure 5: Effect of λ_T on radial distribution of swirl ratio and pressure coefficient (static) for each of the three seals tested (Symbols denote data; lines denote fitted distribution for β and calculated distribution for C_p)

Figure 5 illustrates the variation of swirl ratio and static pressure coefficient in the wheel-space with non-dimensional radius at $Re_\phi = 8.17 \times 10^5$ for two values of λ_T and hence Φ_0. The measurement points for the total pressure in the wheel-space (at $z/S = 0.25$) are also shown on the silhouette in the centre of the figure. In all cases ingress occurred with an annulus swirl ratio, $\beta_a = 1.8$, determined from the isentropic velocity triangles. For all seals with $\lambda_T = 0$, there is no superposed flow and the core rotation $\beta = 0.44$ is observed for $r/b < 0.8$. The swirl ratio at the larger radii outside of the core region increases radially outward with the influence of highly swirling ingested flow. The case $\lambda_T = 0$ has the maximum ingress and the concentration effectiveness everywhere in the wheel-space is zero. Increasing the sealing flow caused a reduction in the core rotation as the wheel-space pressurised. The level of swirl at the periphery of the wheel-space also reduced as the increased sealant flow decreased ingestion from the annulus. As discussed above, at common values of λ_T there are significant differences in the amount of ingress between the single and double seals. Despite this, the swirl ratios in the inner wheel-space for the two cases are similar, illustrating that β is governed principally by λ_T. The exception to this trend is at $r/b = 0.875$ where local effects of the lower portion of the rotating radial seal are observed for the double seal. In the outer wheel-space the swirl is seen to increase rapidly with radius from $\beta \approx 0.44$ to $\beta \approx 0.86$ for the $\lambda_T = 0$ case under the influence of highly swirling ingested flow.

Consider now the variation of C_p in the wheel-space, shown on the right hand side of Figure 5. For a rotating inviscid core, the radial momentum equation reduces to a balance between the pressure force and the centripetal acceleration so that:

$$\frac{1}{\rho}\frac{dp}{dr} = \frac{V_\phi^2}{r}$$

Using the definitions of C_p and β, the equation can be integrated to give:

8

$$C_p = \frac{p - p_{ref}}{0.5\rho\,\Omega^2 b^2} = 2\int_{x_{ref}}^{x} x\beta^2\,dx$$

where p_{ref} is the pressure at $x = r/b = x_{ref}$; for the results presented here, $x_{ref} = 0.6$. The numerical integration was carried out using Simpson's rule, with values of β obtained from a least-squares cubic spline fitted to the experimental data.

The results for the single seals and the inner wheel-space of the double seal ($r/b < 0.9$) show very good agreement between the calculated and measured distributions of C_p. This shows that the radial distribution of the swirl ratio determines the radial distribution of pressure in the wheel-space.

In the outer wheel-space of the double seal ($r/b > 0.9$) the geometric features, as well as the ingress into the intermediate annulus, have affected the distribution of swirl and pressure. The calculated and measured distributions of C_p are therefore no longer in agreement.

A detailed discussion on the effect of ingestion on the internal fluid dynamics of the wheel-space is presented in Sangan *et al.* (2014).

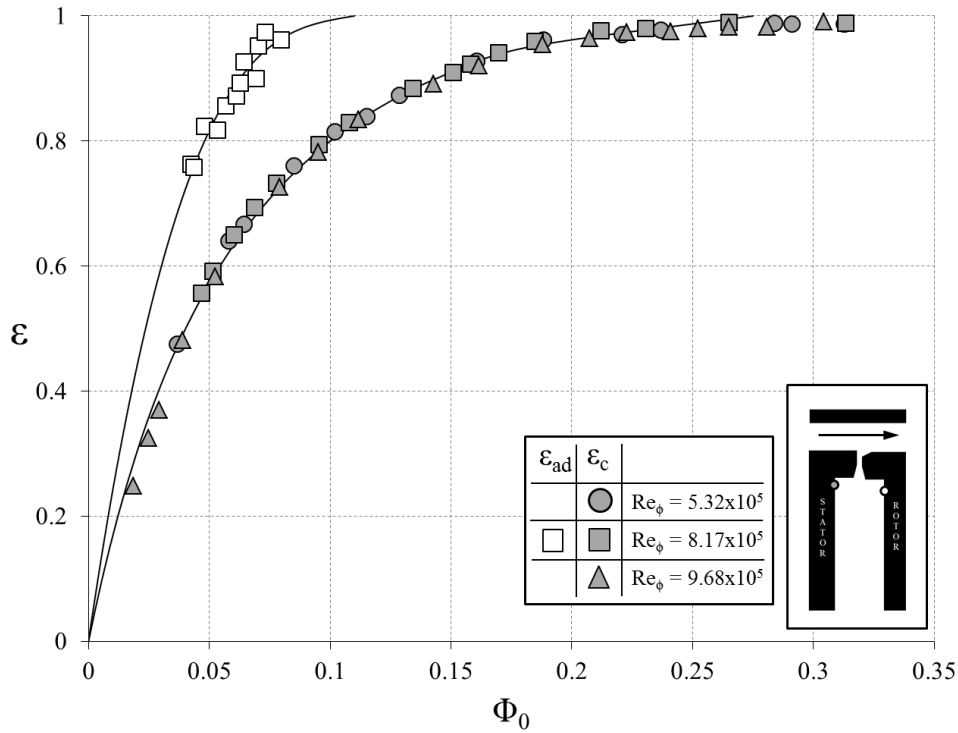**Variation of Effectiveness with Sealant Flow Rate**
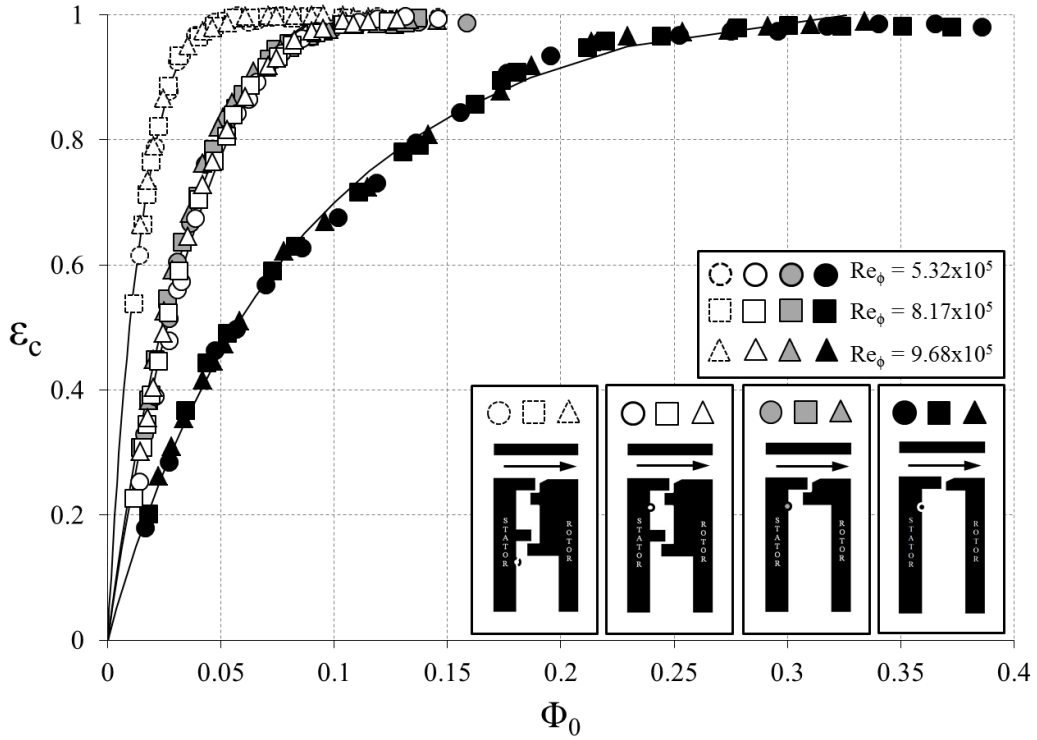
Figure 6: Variation of ε_c with sealant flow rate for each of the three seals tested (Symbols denote data; lines are theoretical curves)

Figure 6 shows the variation of measured concentration effectiveness for the axial-clearance, radial-clearance and double radial-clearance seals plotted versus Φ_0. The effectiveness values for the single seals were based on the concentration measurements made on the stator surface at $r/b = 0.958$. For the double seal, the effectiveness was determined in the inner wheel-space at $r/b = 0.85$ and in the outer wheel-space at $r/b = 0.958$. The figure illustrates that ε_c increases with increasing Φ_0, as the sealing flow pressurises the wheel-space and reduces ingestion through the rim-seal. The data collapses onto a single curve, which is independent of rotational Reynolds number, Re_ϕ.

As revealed in Figure 4, in the outer wheel-space the effectiveness for the single radial-clearance seal and the double seal is unchanged. However, in the inner wheel-space the effectiveness of the double seal is significantly higher; that is, sealing the inner wheel-space requires approximately 50% of the air required to prevent ingress through the outer seal.

Also shown in Figure 6 are the theoretical effectiveness curves based on the orifice model developed by Owen (2011). The model provides an estimate of the minimum non-dimensional sealing flow rate required to prevent ingestion, Φ_{min}, and the ratio of the rim-seal discharge coefficients, Γ_c. As no previous knowledge of the pressure distribution in the annulus is required, or the associated discharge coefficients, the orifice model is a powerful tool for rim-seal design. The equations are fitted to the experimental data using the maximum likelihood method described by Zhou *et al.* (2013). For all seals the experimental data are in good agreement with the theoretical curve.

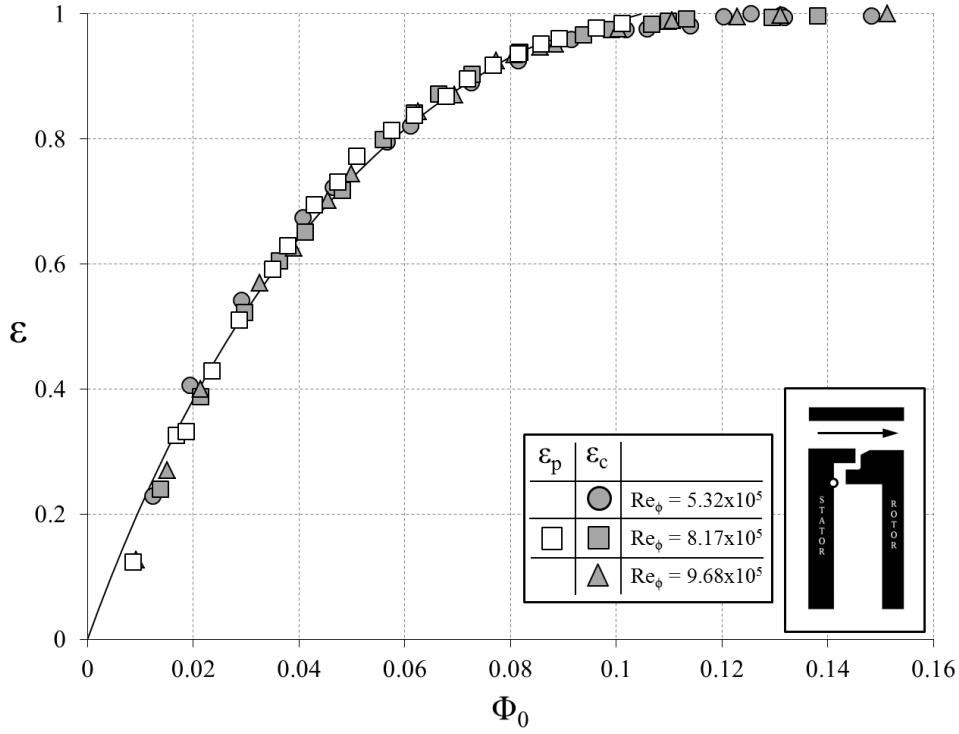**Effectiveness Measurments on the Rotor Surface**

Figure 7: Variation of adiabatic and concentration effectiveness with sealant flow rate (Symbols denote data; lines are theoretical curves)

As one of the most highly stressed components in the turbine, the designer must ensure the integrity of the rotor disc is not compromised when it is exposed to ingested hot mainstream gas. In practice it is not possible to conduct measurements of concentration to determine effectiveness on a rotating surface without the complexity of slip-rings. Consequently, thermochromic liquid crystal (TLC) was used to measure the surface temperature of the rotating disc in a transient experiment to determine the adiabatic effectiveness, ε_{ad}.

Figure 7 shows the comparison between the adiabatic and concentration effectiveness for a derivative of the axial-clearance seal, at the design condition; to reduce heat loss, polycarbonate inserts were attached to the inner surfaces of the aluminium vane and vane platforms in this instance. When ingress occurred the adiabatic effectiveness on the rotor was significantly higher than the sealing effectiveness, ε_c. The boundary layer on the rotor produces a thermal buffer, similar to that created by film cooling on stationary surfaces, which helps to protect the rotor from the ingested fluid.

The effect of the thermal buffer ratio and ingestion on temperature of turbine discs is investigated further by Pountney *et al.* (2013). As far as the authors are aware, this is the first published study on the effect of ingress on the adiabatic temperature of a turbine disc.

Effectiveness Determined by Pressure Measurements

Figure 8: Variation of pressure and concentration effectiveness with sealant flow rate (Symbols denote data; line is theoretical curves)

In a gas turbine the flow rate of the sealing air is controlled by the pressure difference between the compressor outlet and the mainstream annulus near the seal clearance. As in Figure 4 and Figure 6, concentration measurements are widely used in experimental rigs to determine the sealing effectiveness of rim seals as a function of the sealing flow rate. However, for these concentration measurements to be of use to the designers of internal-air systems in engines, it is necessary to relate the sealing effectiveness in terms of the appropriate pressure difference across the rim seal.

A nondimensional pressure difference was determined from measurements at an arbitrary location in the annulus, and at $r/b = 0.958$ in the wheel-space. Owen *et al.* (2014) developed a theoretical model to relate these measurements to the location of mathematical consistency where ε_p is equal to ε_c. The experimental measurements showed that the nondimensional pressure difference at the *sweet spot*, determined from the orifice model fit of the concentration data, varied linearly with the measured nondimensional pressure. Linear regression of this relationship was used to determine the variation of ε_p with sealing flow rate.

Figure 8 shows the variation of sealing effectiveness determined from both pressure and concentration measurements with Φ_o for a radial-clearance rim seal. The calculated values of ε_p were in good agreement with the measured values of ε_c and with the effectiveness equation derived from the orifice model.

Owen *et al.* (2014) also presented steady 3D computations which revealed the location of the *sweet spot* to be very close to the upstream edge of the seal clearance. This location of consistency was shown to be invariant with sealing flow rate for the conditions investigated. A method for extrapolating experimentally-measured effectiveness to a gas turbine engine with similar seal geometry was also proposed.

CONCLUSIONS

This paper provides an overview of experimental results from a research facility which models hot gas ingestion into the wheel-space of an axial turbine stage. Measurements of pressure, CO_2 gas concentration, temperature and swirl were used to assess the performance of different seal designs. The fundamental fluid dynamics associated with ingress has been investigated, and used to explain the improvement in performance of different rim-seal designs. Although the ingestion through the rim seal is a consequence of an unsteady, three-dimensional flow field, and the cause-effect relationship between pressure and the sealing effectiveness is complex, the experimental data is shown to be successfully calculated by simple effectiveness equations developed from a theoretical orifice model.

On the surface of the rotor, an adiabatic effectiveness based on temperature measurements was defined. When ingress occurred, the adiabatic effectiveness was significantly higher than the concentration effectiveness measured on the stator side. The boundary layer on the rotor was shown to produce a thermal buffer which helps protect the surface from the ingested fluid.

As shown by the orifice model equations, externally induced ingress in gas turbines is controlled by the peak-to-trough pressure difference near the rim seal. Measurements made on an experimental rig can be used to determine Φ_{min} and Γ_c for a particular value of ΔC_p. In principle, and within the limits of dimensional similitude, these values should apply to a geometrically-similar engine at the same operating conditions. However, the conditions – particularly the Mach number and temperatures – in engines are usually significantly different from those in experimental rigs. Also, the design codes used for internal air systems usually estimate ingress from pressures rather than gas concentration. A theoretical model was developed which ensures consistency between effectiveness measured by concentration and by pressure. The model introduces the concept of a *sweet spot* location in the annulus where pressures should be resolved to allow the extrapolation from rig to engine to take place.

REFERENCES

Sangan, C. M., Pountney, O. J., Zhou, K., Wilson, M., Owen, J. M., and Lock, G. D., (2013a), "Experimental Measurements of Ingestion through Turbine Rim Seals. Part 1: Externally-Induced Ingress," ASME J. Turbomach., 135, p.021012.

Sangan, C. M., Pountney, O. J., Zhou, K., Wilson, M., Owen, J. M., and Lock, G. D., (2013b), "Experimental Measurements of Ingestion through Turbine Rim Seals. Part 2: Rotationally-Induced Ingress," ASME J. Turbomach., 135, p.021013.

Sangan, C. M., Scobie, J. A., Owen, J. M., Lock, G. D., Tham, K-M., and Laurello, V.P., (2014), "Performance of a Finned Turbine Rim Seal," ASME J. Turbomach., 136, p.111008.

Owen, J. M. and Rogers, R. H., (1989), Flow and heat transfer in rotating-disc systems, Volume 1: Rotor-stator systems, Taunton: Research Studies Press Ltd.

Owen, J. M., Wu, K., Scobie, J. A., Sangan, C. M., Cho, G., and Lock, G. D., (2014), "Use of Pressure Measurements to Determine Effectiveness of Turbine Rim Seals," ASME Paper GT2014-25200. To appear in ASME J. Gas Turb. Power.

Pountney, O. J., Sangan, C. M., Lock, G. D. and Owen, J. M., (2013), "Effect of Ingestion on Temperature of Turbine Discs," ASME J. Turbomach., 135, p. 051010.

Owen, J. M., (2011), "Prediction of Ingestion through Turbine Rim Seals. Part II: Externally Induced and Combined Ingress," ASME J. Turbomach., 133(3), pp. 031006.

Sangan, C. M., Pountney, O. J., Scobie, J.A., Wilson, M., Owen, J. M., and Lock, G. D., (2013c), "Experimental Measurements of Ingestion Through Turbine Rim Seals. Part 3: Single and Double Seals," ASME J. Turbomach., 135, p.051011.

Sangan, C. M., Lalwani, Y., Owen, J. M., and Lock, G. D., (2014), "Fluid Dynamics of a Gas Turbine Wheel-space with Ingestion", Proceedings of the Institution of Mechanical Engineers Part A: Journal of Power and Energy, 228 (5), pp. 508-524.

Zhou, K., Wood, S. N., and Owen, J. M., (2013), "Statistical and Theoretical Models of Ingestion through Turbine Rim Seals," ASME J. Turbomach., 135, p.021014.